JOURNAL OF THE ROYAL SOCIETY Interface

rsif.royalsocietypublishing.org

Research

Cite this article: Chen Y, Shih M-C, Wu M-H, Yang E-C, Chi K-J. 2014 Underwater attachment using hairs: the functioning of spatula and sucker setae from male diving beetles. *J. R. Soc. Interface* **11**: 20140273. http://dx.doi.org/10.1098/rsif.2014.0273

Received: 14 March 2014
Accepted: 21 May 2014

Subject Areas:
biomechanics, biomimetics, biophysics

Keywords:
diving beetles, underwater attachment, biofibrillar adhesives, suction, viscous adhesion, attachment–detachment process

Author for correspondence:
Kai-Jung Chi
e-mail: kjchi@phys.nchu.edu.tw

Electronic supplementary material is available at http://dx.doi.org/10.1098/rsif.2014.0273 or via http://rsif.royalsocietypublishing.org.

Royal Society Publishing

Underwater attachment using hairs: the functioning of spatula and sucker setae from male diving beetles

Ying Chen[1], Ming-Chih Shih[1], Ming-Huang Wu[1], En-Cheng Yang[3] and Kai-Jung Chi[1,2]

[1]Department of Physics and Institute of Biophysics, and [2]Department of Life Sciences, National Chung Hsing University, Taichung 40227, Taiwan
[3]Department of Entomology, National Taiwan University, Taipei 10617, Taiwan

Males of Dytiscinae beetles use specialized adhesive setae to adhere to female elytra during underwater courtship. This coevolution of male setae and female elytra has attracted much attention since Darwin. However, there has been little examination of their biomechanical functioning despite increasing knowledge on biofibrillar adhesion. Here, we report and compare, for the first time, the mechanisms of underwater attachment using two hair types, the primitive spatula and derived 'passive' sucker, found in male diving beetles. Results from interspecific scaling of protarsal palettes and adhesion by single seta suggest better performance in the later-evolved circular (sucker) setae. Spatula setae with a modified shallow sucker and channels use the combined mechanisms of suction and viscous resistance for adhesion. Velocity-dependent adhesion provides sufficient control for resisting the female's erratic movements while also detaching easily through slow peeling. Direction-dependent shear resistance helps reorient setae surfaces into a preferred direction for effective adhesion. Seta deformation using different mechanisms for circular and spatula setae reduces the force that is transmitted to the contact interface. A softer spring in spatula setae explains their adhesion at lower preloads and assists in complete substrate contact. Attachment mechanisms revealed in adhesive setae with modified spatula and passive suckers provide insights for bioinspired designs of underwater attachment devices.

1. Introduction

The ability to attach to surfaces plays an essential role in the lives of many animals [1]. Attachments can be permanent via chemical adhesives [2,3] or temporary during locomotion, predation, copulation or even pollination [4,5]. Diverse attachment devices have evolved independently in different groups of animals and are classified according to their functional mechanisms. The forces involved depend on the scale of the two contact surfaces and can include suction, mechanical interlocking, friction, electrostatic forces, van der Waals forces, chemical bonding and even capillary effects and viscous forces [5–7]. Since the effects of van der Waals interaction were demonstrated in the adhesion of gecko spatula setae [8], much attention has been drawn to the functional mechanisms and biomimetic applications of these nanoscale fibrillar adhesives [9,10].

The contact geometry of biological fibrillar adhesives evolved independently between and across broad size ranges of animals and has a strong effect on adhesion [11,12]. Among various fibrillar forms, mushroom- and spatula-shaped contact elements are most commonly found at both macro- and microscopical scales [13]. Spatula setae require a shear force to generate adhesion and are most often involved in short-term temporary adhesion during locomotion because of their strong adhesion through intimate contact with the substrate, fast contact breakage by peeling, self-cleaning and low

dependence on substrate chemistry. Heavier animals or those relying mainly on dry adhesion tend to have smaller and more densely packed terminal contacts [14] to increase the total peeling line for greater attachment force [15]. By contrast, mushroom-shaped setae can stay adhered without any external force and require high pull-off forces to rupture the contact; therefore, they are optimal for prolonged attachment in challenging environments or during the pairing process [12,13]. A thorough understanding of the morphology, physical mechanisms or even the scaling effects of these adhesive hairs allows further examination of their interactions with varying substrates and provides insights for the bioinspired design of artificial adhesives.

To date, mechanisms for underwater attachment remain little explored. Besides mechanical interlocking (e.g. mayfly larvae [16]) and chemical bonding (e.g. mussels [17]), the pressure difference provided by suckers is widely used. Cephalopods use arm and tentacle suckers for prey capture or manipulation by varying the pressure differential through active muscle control [18–21]. Muscular suckers also evolved in some fishes as oral discs to maintain position [22,23] or at modified dorsal fins to attach to a host's skin [24]. Despite the growing knowledge of dry adhesion in biological fibrillar systems, little is known about their underwater attachment except for a few demonstrations of bioinspired fibrillar adhesives with chemical coatings [9] or through a suction effect [25,26].

Diving beetles (Dytiscidae) are aquatic insects that store air underneath their elytra for respiration and have hairy, paddle-like hind legs for swimming [27,28]. During precopulatory courtship, the male uses its forelegs to mount on the female's elytra, but mating cannot proceed unless the male manages to manoeuvre to the correct position [29]. The forelegs and elytra provide a striking example of sexual dimorphism [30,31]. Male forelegs have enlarged protarsomeres (the protarsal palettes) with modified adhesive setae either in spatula or sucker form, and female elytra commonly have rough surface structures to aid the male in mounting, as suggested by Darwin [32]. However, a recent biomechanical study shows that the rough structure instead deteriorates the adhesion of male palette suckers [33]. Therefore, continuous morphological modifications of female elytra and male attachment devices throughout the evolution of diving beetles may instead suggest sexual conflict and an arms race between the two sexes [30,34,35]. Females might also use erratic swimming behaviours to dislodge the mounted male to avoid depletion of stored oxygen and for mate choice during courtship.

Biological fibrillar adhesives with terminal contacts shaped like suckers as found in some male diving beetles are unique among insects. Phylogenetic studies [30,35] suggest that sucker setae in males evolved a single time within the subfamily Dytiscinae. Most other dytiscid taxa, including the Cybistrini, the sister group to other Dytiscinae, instead have adhesive setae with spatula-shaped apices that are more commonly found among other insects [12]. Previous studies suggest that the whole palette with sucker setae generates adhesive forces about four times the body weight [36] and performs better on smooth female elytra than on rough ones [33]. A palette with spatula setae has better adhesion on wet surfaces than dry and can generate even stronger shear resistance than adhesion [37,38]. The attachment performance of a single seta has only been examined on sucker setae [36].

Ever since Darwin, sexually dimorphic forelegs and elytra of diving beetles have been used to study the evolutionary process of sexual conflict and the coevolutionary arms race between the sexes [30,34,35]. However, less is known about the biomechanics of their specialized attachment devices, either in the primitive spatula form or the derived sucker form. Spatula setae found in insects are mostly used for dry adhesion involving a van der Waals interaction or wet adhesion using capillary force [12], whereas biological suckers mostly require muscular control for sealing and generating pressure differences [18,19,22–24]. Therefore, members of the Dytiscinae provide us with a great opportunity to explore and compare the functional mechanisms of spatula setae and 'passive' suckers for underwater adhesion. To this end, we (i) investigated scaling relationships between palette size and body size among species with different seta types, (ii) measured the adhesive force and shear resistance generated by a single seta, estimated overall performance and examined the effects of preloading, pull-off velocity and shearing directions, (iii) associated seta morphology and the attachment–detachment process with its attachment mechanics and (iv) propose novel mechanisms for underwater attachment using fibrillar systems.

2. Methods

2.1. Scaling of protarsal palettes

We used 28 live samples and 41 museum specimens to investigate how protarsal palette size varies with body size in male diving beetles. Because body mass (M_B) was unavailable from museum records, we instead measured the body area (A_B) of the specimens and estimated their M_B using the $A_B - M_B$ relationship obtained empirically from live subjects. Live males of four species were collected from the field, among which three have sucker setae (*Eretes sticticus*, *Hydaticus vittatus* and *Hydaticus pacificus*) and one has spatula setae (*Cybister rugosus*). Each subject was weighed and photographed from a dorsal view, and palettes were photographed from a ventral view. The body length (L_B), body width (W_B), body area (A_B) and palette area (A_P; figure 1*a*,*b*,*g*) were calculated from the photographs using ImageJ (National Institutes of Health, Bethesda, MD, USA). For the dytiscid specimens from the National Museum of Natural Science (NMNS) in Taichung, Taiwan, body size (L_B, W_B, A_B) and A_P were calculated following the same procedures for live samples. Information about the museum specimens is summarized in the electronic supplementary material, table S1.

2.2. Morphology of palettes and adhesive setae

A ventral view of each palette from *H. pacificus* (with sucker setae) or *C. rugosus* (with spatula setae), lightly attached to the coverslip, was first examined under an optical stereomicroscope to calculate seta numbers and seta area (A_{ST}; figure 1*d*,*g*). Seta surface morphology was examined using a scanning electron microscope (SEM; JSM-5600; Japan Electron Optics Laboratory Co., Tokyo, Japan). Because a shallow sucker is found beneath the stalk of the spatula seta from *C. rugosus* (figure 1*d*,*e*), in the rest of this paper, we use 'circular seta' to refer to the 'sucker seta' of previous studies. The dimensions of surface structures from two species were measured from SEM images (figure 1*f*,*i*).

2.3. Adhesive and shear forces of a single seta

We collected live adult male *H. pacificus* (0.252 ± 0.015 g; $n = 8$) and *C. rugosus* (2.044 ± 0.377 g; $n = 12$) diving beetles from

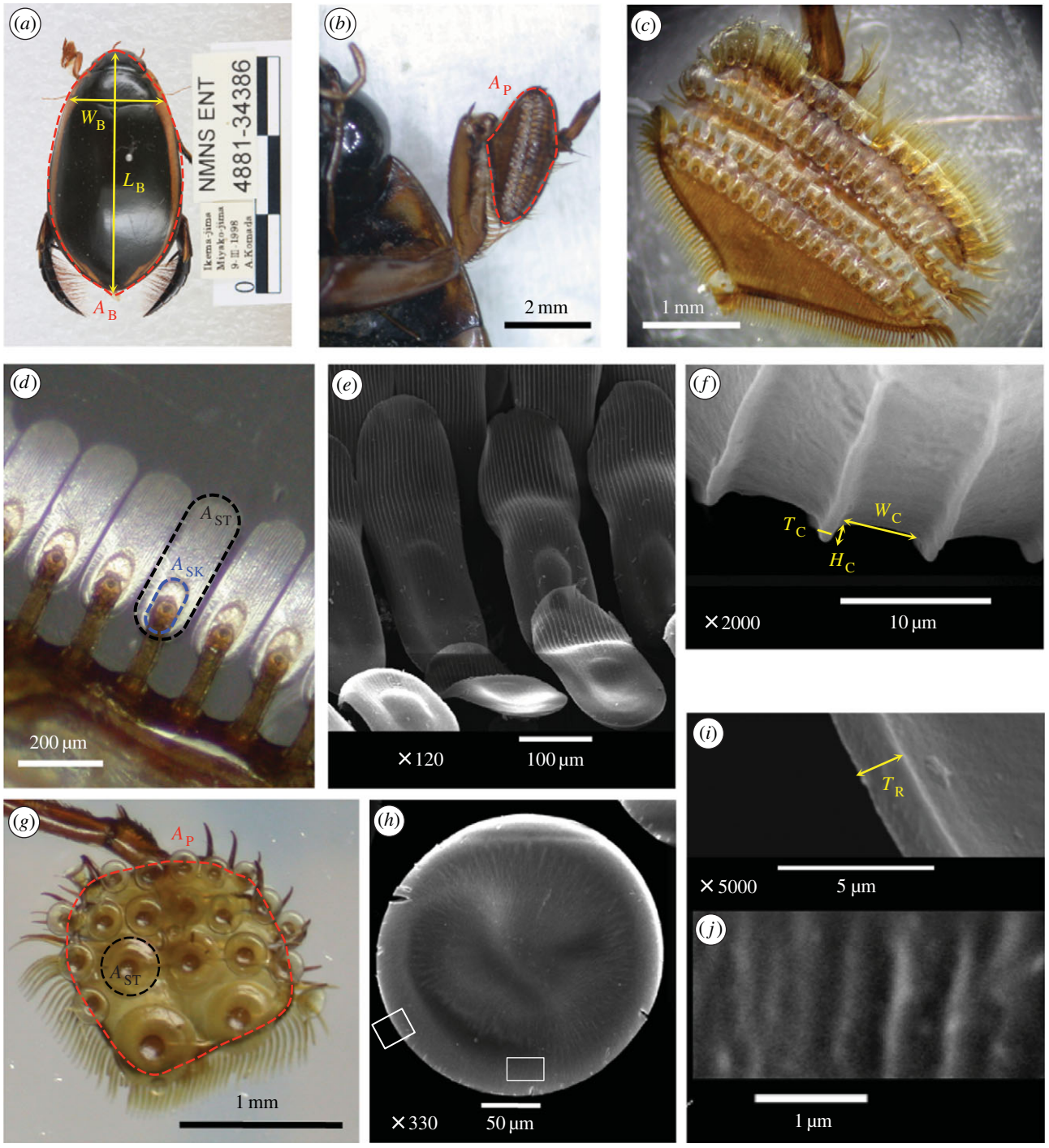

Figure 1. Adhesive devices of male diving beetles. (*a*) Measurement of the body length (L_B), body width (W_B) and body area (A_B; area enclosed by the red dashed line) of a male diving beetle. (*b–f*) In male *C. rugosus*, the proleg has an expanded palette (*b*,*c*) composed of protarsomeres bearing specialized adhesive setae on their ventral side. Each spatula seta connects to the palette with an off-centre stalk (*d*) and its ventral surface has an oval-shaped sucker (blue dashed line) from which parallel channels extend distally (*e*). Channel width (W_C), channel height (H_C) and channel wall thickness (T_C) can be measured from (*f*). (*g–j*) By contrast, the proleg of male *H. pacificus* has one round palette with circular setae (*g*,*h*). Enlargements of white boxes in (*h*) show that the circular seta has a rim on its edge with thickness (T_R) (i), although with a rough ventral surface it does not have distinct channels as found on spatula setae (*j*). Area of the palette (A_P; red in *b*,*g*), seta (A_{ST}; black in *d*,*g*) or spatula sucker (A_{SK}; blue in *d*) is the area enclosed by the dashed line. (*a–d*,*g*) Light micrographs; (*e*,*f*,*h–j*) Scanning electron micrographs.

ponds in Pingtung, Yunlin and Taoyuan Counties in Taiwan (table 1). All subjects were maintained in a laboratory tank at 25°C with a photoperiod of 13 L : 11 D. Prior to the experiments, the subject was anaesthetized on ice for 10 min until immobile. Isolated palette samples were kept in double-distilled water and cleaned ultrasonically for 1 h. Single seta was prepared for testing by cutting the palette into small pieces, removing extra setae and mounting the sample onto the tip of an insect pin with Super Glue (3M Co., St Paul, MN, USA). Each sample was examined under an optical stereomicroscope, and only successfully prepared samples were used for force measurement. In total, we prepared 34 circular seta samples (*H. pacificus*, $n = 8$) and 45 spatula seta samples (*C. rugosus*, $n = 12$). Prior to testing the attachments, the ventral view of the sample's contact surface, lightly attached to the coverslip, was photographed for later calculation of its A_{ST}.

The set-up for measuring adhesive and shear forces was composed of a motorized stage, a glass substrate and a force measurement system (figure 2*a*,*b*). The substrate was mounted at the bottom of a 1.5 × 1.5 cm plastic box, filled with double-distilled

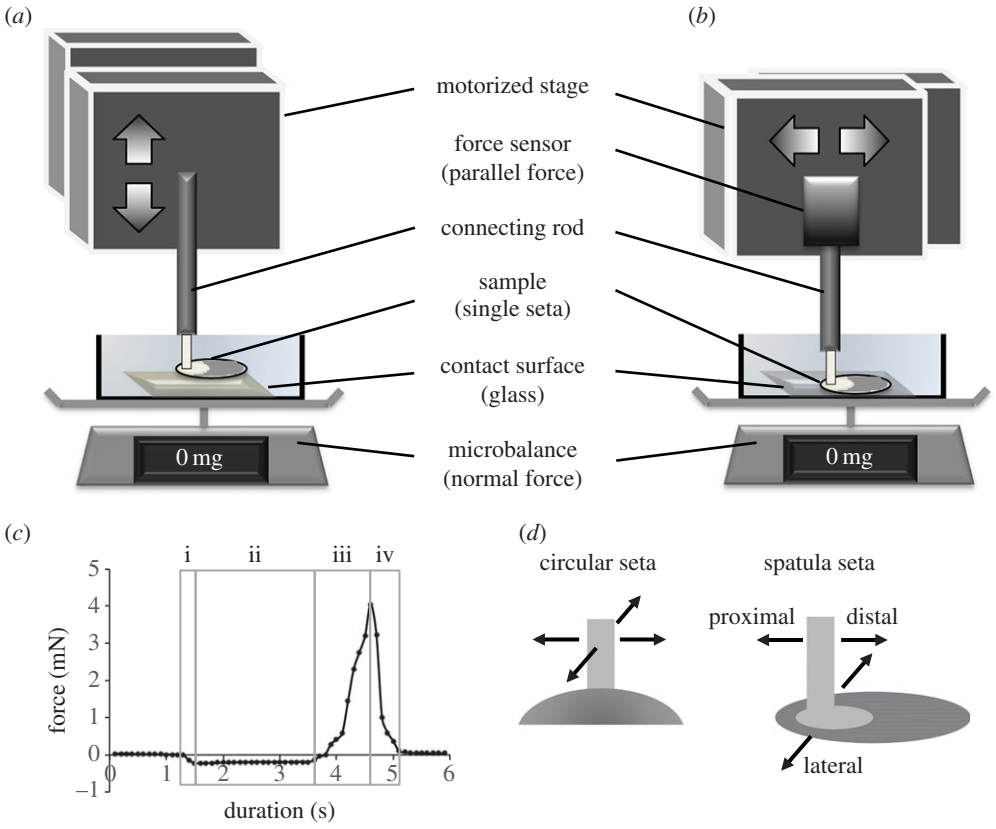

Figure 2. Measurement of the attachment force of a single adhesive seta. (*a*,*b*) Experimental set-ups for measuring adhesive and shear forces, respectively. The vertical force was measured using a microbalance, whereas horizontal shear resistance was measured using a force sensor. (*c*) Force was recorded throughout the attachment and detachment cycle of a seta sample. The preload includes stages i and ii, and the pull-off includes stages iii and iv. The adhesive force generated by a seta can be quantified as the maximum pull-off force. (*d*) Shearing directions for the test sample. The circular seta (left) is tested in two perpendicular directions; the spatula seta (right) is tested in distal, proximal and lateral directions with respect to the seta contact. (Online version in colour.)

Table 1. Summary of body size and seta information of live male diving beetles used for scaling analyses. M_B, body mass; L_B, body length; W_B, body width; and A_B, body area from top view.

species	seta type	*n*	M_B (g)	L_B (mm)	W_B (mm)	A_B (mm^2)	seta nos per palette
E. sticticus	circular	2	0.142 ± 0.010	13.0 ± 1.2	5.4 ± 1.0	52 ± 16	—[a]
H. vittatus	circular	6	0.136 ± 0.014	12.6 ± 0.5	5.2 ± 0.3	64 ± 3	~20
H. pacificus	circular	8	0.252 ± 0.015	15.8 ± 0.3	7.0 ± 0.2	101 ± 6	22
C. rugosus	spatula	12	2.044 ± 0.377	31.3 ± 0.8	12.6 ± 0.8	411 ± 49	85

[a]The palette of *E. sticticus* has one big sucker at its proximal end and many small suckers that were too small to count in the images.

water and placed on a microbalance. The motorized stage (T-LSM025A, Zaber Technologies, Richmond, BC, Canada) moves samples in three orthogonal directions controlled by a custom-made program in LabView (National Instruments, Austin, TX, USA). In this study, the origin is defined as the position where the seta comes completely into contact with the substrate at initial preloading; therefore, position data can provide information on seta deformation. Vertical motion leads to seta preloading or pull-off, and the normal force can be recorded from the microbalance (XS105; Mettler Toledo, Hightstown, NJ, USA) using the LabView program with a precision of 0.01 mg at a sampling rate of 10 Hz (figure 2*a*). Lateral motion leads to the shearing of seta relative to the substrate, and the resistance to this can be measured using a force sensor (LSB200 10 g S-beam load cell, Futek Advanced Sensor Technology, Irvine, CA, USA) mounted on the side of the motorized stage (figure 2*b*). The signal was sampled at 100 Hz using an I/O board (USB X-series 6341, National Instruments, Austin, TX, USA), and the voltage output was amplified using a signal conditioner (CSG110, Futek Advanced Sensor Technology). To remove high-frequency noises, we used a custom spline-smoothing algorithm provided by LabView. Because the attachment force results from the resistance of the seta–substrate interface to pulling, it can be quantified from the force trace recorded during the attachment–detachment process (figure 2*c*). Each test event was filmed laterally at 24 frames per second (fps) using a digital camera (Nikon D90, Nikon Co., Tokyo, Japan) through an optical stereomicroscope placed perpendicular to the plane of seta motion.

Seta samples maintained their adhesion ability after multiple attachment cycles; therefore, each was tested under three to five loading conditions, with a 5 s interval between two consecutive tests. To evaluate the effect of multiple testing, we used seven samples from each seta type and conducted repeats on each sample under identical test conditions. Repeatability of attachment performance was assessed for each sample using relative standard deviation (RSD), i.e. the ratio of the standard deviation

to its mean, in percentage. A lower value of RSD indicates a lower variability and hence greater repeatability among the measurements. Because the RSD for the tested samples is $3.85 \pm 2.33\%$ for circular setae and $3.11 \pm 1.36\%$ for spatula setae ($n = 7$ for each type), both lower than 5% from the mean, we considered our test results reliable even after multiple tests. Three replications under each test condition were averaged for further analyses. To examine the effects of preloading, we collected eight circular setae from two subjects and 12 spatula setae from six subjects, and tested each one under three to five different preloads ranging from 0.2 to 4 mN. These tests were conducted at a pull-off velocity of 150 $\mu m\ s^{-1}$, which generated the best attachment performances in preliminary tests. To determine the effects of pull-off velocity, we tested five circular setae and six spatula setae, collected from different subjects, at a preload of 1 mN with varying pull-off velocities ranging from 15 to 375 $\mu m\ s^{-1}$. For the effects of seta size, samples of different sizes were tested at different preloads at a pull-off velocity of 150 $\mu m\ s^{-1}$, with the best performances being used for analyses. To assess the effects of shape symmetry, we measured the shear resistance of each seta under three to four preloads ranging between 0.2 and 2 mN at a constant sliding velocity of 150 $\mu m\ s^{-1}$ (figure 2*d*). For spatula setae, eight samples were collected from five subjects, and each seta was tested in three shearing directions: distal (i.e. seta sliding away from the stalk), proximal (i.e. seta sliding toward the stalk) and lateral (i.e. seta sliding perpendicular to the long axis of the seta contact). For radially symmetric circular setae, five samples from two beetles were subjected to a sliding motion applied in two perpendicular directions.

2.4. Statistical analyses

We conducted a *t*-test to compare functional preload and attachment performances between circular and spatula setae. An analysis of variance (ANOVA) was used to test whether adhesive capability varies with different pull-off velocities. An ordinary least-squares (OLS) regression was used to obtain the scaling relationships of body and palette sizes and to examine the effects of seta area, preloading, pull-off velocity and shearing direction on the attachment performance of circular and spatula setae. Different testing conditions on the same test sample were considered independent trials. To compare between OLS regression lines, we conducted an analysis of covariance (ANCOVA). For all tests, samples were considered significantly different if $p < 0.05$.

3. Results

3.1. Scaling of protarsal palettes

Table 1 summarizes body sizes and numbers of adhesive setae of live males of *E. sticticus*, *H. vittatus*, *H. pacificus* (with circular setae) and *C. rugosus* (with spatula setae). The relationship between the A_B and M_B of these live males is presented in figure 3*a*, and a scaling factor $b \sim 0.67$ suggests isometry (or similar body shape) between these four species (electronic supplementary material, table S2). The scaling of palette size with body size was examined using museum specimens. The relationship between A_P and M_B, where M_B was estimated from the $A_B - M_B$ relationship in figure 3*a*, could be obtained for each type of seta (figure 3*b*). ANCOVA suggests significantly different OLS regression lines for each seta type (slopes: $F_{1,37} = 1.93$, $p = 0.17$; intercepts: $F_{1,38} = 51.45$, $p < 0.0001$) but with a common slope of 0.78 (electronic supplementary material, table S2). Therefore, at any given body mass, the area of palettes with spatula setae is smaller than with circular setae. However, among the largest samples collected, the palettes with either type of setae have similar sizes. All scaling relationships and ANCOVA results are summarized in the electronic supplementary material, table S2.

3.2. Morphology of palettes and adhesive setae

The forelegs of male *C. rugosus* have expanded oval-shaped palettes composed of three protarsomeres bearing setae on their ventral side (figure 1*b*,*c*). Three types of setae were identified: long setae along the palette edge, short setae at the proximal end and specialized spatulate adhesive setae aligned in four rows (figure 1*c*,*d*). A spatula seta has a contact surface of about 400×150 μm in size (figure 1*d*) and a stalk approximately 250 μm in length connected to the palette (figures 1*d* and 5*b*). The contact surface directly under the stalk has an oval sucker from which parallel channels approximately 5 μm in width and approximately 3 μm in height extend distally (figure 1*e*,*f*). The channels are equally spaced and have wall thickness of 1–2 μm. By contrast, the three protarsomeres of male *H. pacificus* are merged into a single round palette with adhesive circular setae in suction-cup form, its A_{ST} ranging from 0.020 to 0.240 mm^2 (figure 1*g*,*h* and table 2). Each circular seta has a rim approximately 1.5 μm thick and a stalk connecting it to the palette, and its ventral surface has shallow grooves arranged radially (figures 1*i*,*j* and 5*a*).

3.3. Attachment performance of single seta: circular versus spatula

On average, the areas of both types of setae are similar, but the circular setae of *H. pacificus* have a wider size range (table 2). OLS regressions show that the adhesive force (F_a) generated by a single circular seta strongly depends on A_{ST} ($r^2 = 0.94$, $p < 0.0001$; $n = 9$), but in the spatula setae of *C. rugosus*, no significance is found ($r^2 = 0.24$, $p = 0.1287$; $n = 12$; figure 3*c* and electronic supplementary material, table S2). ANCOVA suggests there is no significant difference between regression lines of these two seta types (slopes: $F_{1,16} = 0.31$, $p = 0.58$; intercept: $F_{1,17} = 3.12$, $p = 0.10$; electronic supplementary material, table S2); therefore, among tested samples, the $F_a - A_{ST}$ relationship for the two types of setae can be described using a new regression line: $\log F_a = 0.86 \log A_{ST} + 1.57$. In spatula setae, no adhesive force could be measured when only the channel region was in contact with the substrate. If we consider the 'sucker' as the effective attachment surface, a spatula seta could generate similar adhesive force with less area than a circular seta (figure 3*c*).

3.3.1. Load-dependence in adhesion

To assess and compare adhesive performance between two types of setae, we normalized the adhesive force to the area of a single seta (F_a/A_{ST}). For circular setae, this 'adhesive stress' increased with preloading up to 2.5–3.0 mN, whereas spatula setae reached their maximums at a preloading of approximately 1.0 mN and decreased at greater loads (figure 4*a*). Within the range of positive preloading effects, ANCOVA suggests significantly different OLS regression lines for the two seta types (slopes: $F_{1,70} = 8.53$, $p = 0.0047$; electronic supplementary material, table S3). Considering only the sucker area, the adhesive stress of spatula setae would be approximately four times greater (figure 4*a*). The effective preloadings and adhesive stresses for both types of setae are summarized in table 2; on

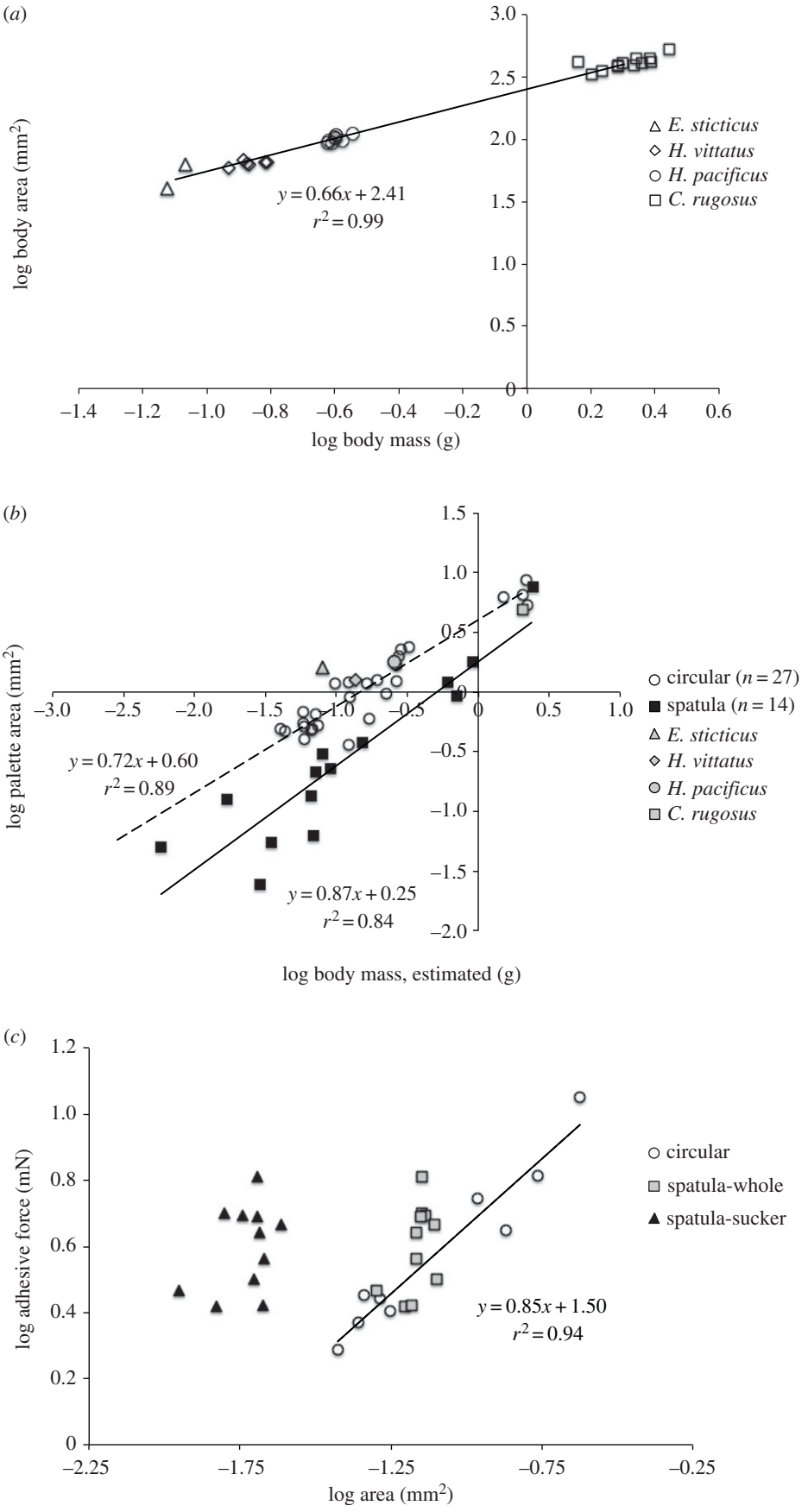

Figure 3. Scaling of body size, palette size and setae adhesive forces in male diving beetles. (*a*) Relationship between body area and body mass of live male diving beetles of four species (circular setae, *E. sticticus*, *H. vittatus* and *H. pacificus*; spatula setae, *C. rugosus*). The regression line shows the interspecific relationship. (*b*) Relationship between palette area and body mass of museum specimens with circular (open circle; OLS regression in dashed line) and spatula setae (filled square, OLS regression in solid line). Body mass was estimated using results from (*a*). Results from live samples of four species are also presented (grey symbols). (c) Relationship between adhesive force and area of circular setae (nine samples from *H. pacificus*, $n = 2$) and spatula setae (12 samples from *C. rugosus*, $n = 6$). For the latter, we considered the area for the whole seta and the sucker. Comparisons of OLS regression lines are presented in the electronic supplementary material table S2.

Table 2. Summary of seta area, adhesion and shear attachment performance. A_{ST}, single seta area; F_a, F_s, adhesive and shear forces produced by a single seta, respectively; *BW*, body weight, calculated as body mass (M_B) × gravitational acceleration (g) and has unit of mN in this study. *p-values of *t*-test comparing between circular and spatula setae.

species (seta type)	seta area		adhesion				shear			
	A_{ST}[a] (mm^2)	ΣA_{ST}[b] (mm^2)	preload[c] (mN)	F_a/A_{ST}[c] (kPa)	ΣF_a[d] (mN)	$\Sigma F_a/BW$	preload[e] (mN)	F_s/A_{ST}[e] (kPa)	ΣF_s[d] (mN)	$\Sigma F_s/BW$
H. pacificus (circular)	0.067 ± 0.079 (0.020∼0.240)	2.960 ± 0.512	1.15 ± 0.76	55 ± 17	∼160	∼60	0.69 ± 0.25	30 ± 5.3	∼90	∼35
C. rugosus (spatula)	0.058 ± 0.009	9.889 ± 1.347	0.73 ± 0.31	54 ± 21	∼530	∼25	*d*: 0.78 ± 0.21	9.7 ± 4.2	∼95	∼5
							p: 0.74 ± 0.33	5.2 ± 3.7	∼50	∼2.5
							l: 0.75 ± 0.32	10 ± 5.4	∼100	∼5
*p**			<0.001	0.90			0.40	<0.001		

[a]Calculated from all setae on one palette of each species ($n = 2$ for *H. pacificus*; $n = 6$ for *C. rugosus*).
[b]ΣA_{ST} is the total seta area from two palettes, calculated as twice the sum of all A_{ST} from one palette.
[c]Obtained from data shown in figure 4*a*.
[d]Estimated total forces: $\Sigma F_a = F_a/A_{ST} \times \Sigma A_{ST}$; $\Sigma F_s = F_s/A_{ST} \times \Sigma A_{ST}$.
[e]Obtained from data shown in figure 4*c*.

average, adhesive stress is similar between types but is achieved at significantly lower preloading in spatula setae.

3.3.2. Velocity-dependence in adhesion

The two types of setae responded differently to pull-off velocities, varying between 15 and 375 μm s^{-1} (figure 4*b*). Circular setae reached their maximum adhesion capability (i.e. adhesive force normalized by the best performance of the sample) at pull-off velocities of 51.0 ± 22.1 μm s^{-1} ($n = 5$), but no significant differences were found between 23.0 and 75.0 μm s^{-1} (ANOVA; $F_{3,16} = 1.021$, $p = 0.410$). Performance decreased slightly as pull-off velocity increased and approached equality between 225.0 and 375.0 μm s^{-1} (ANOVA; $F_{2,10} = 1.921$, $p = 0.197$). By contrast, spatula setae had much lower adhesiveness at low pull-off velocities, but their performance was enhanced with increasing velocity and reached its maximum at the significantly greater velocity of 187.5 ± 71.2 μm s^{-1} ($n = 6$). Adhesion performance at even higher velocities was similar (ANOVA; $F_{5,30} = 1.373$, $p = 0.262$). Therefore, spatula setae exhibit velocity-dependent adhesion before reaching their maximum capability.

3.3.3. Direction-dependent resistance to shear

Relationships between shear stress (shear resistance F_s normalized by A_{ST}) and preloading were obtained for different shearing directions (figure 4*c*). For circular setae shearing in either direction, resistance had a non-significant relationship with the preload (OLS regression: $p = 0.38$ and 0.90, respectively). For spatula setae, the preload had significant effects when shearing proximally and distally ($p = 0.0003$ and 0.001, respectively), but the effect was non-significant for lateral shearing ($p = 0.840$; electronic supplementary material, table S3). Functional preloads and shear stresses for single seta are summarized in table 2. In general, the preload is similar, but the shear resistance of circular setae is greater than for spatula setae.

Circular setae show isotropic resistance to shear (ANCOVA, slopes: $F_{1,9} = 0.55$, $p = 0.48$; intercept: $F_{1,10} = 0.68$, $p = 0.43$), whereas spatula setae show directional dependence (ANCOVA, slopes: $F_{2,56} = 4.71$, $p = 0.0128$; electronic supplementary material, table S3 and figure 4*c*). The slopes for the relationship between shear stress and preloading are similar between distal and proximal shearing (ANCOVA, slopes: $F_{1,36} = 2.06$, $p = 0.16$; common slope = 9.79), but distal shearing can generate greater resistance (ANCOVA, intercepts: $F_{1,37} = 20.31$, $p < 0.0001$). Shear resistance measured laterally varied widely but had the greatest values among the three directions tested (figure 4*c*).

3.4. Seta attachment–detachment process

Figure 5 demonstrates the stages of the attachment–detachment processes of a circular seta from *H. pacificus* (figure 5*a*) and a spatula seta from *C. rugosus* (figure 5*b*). For either type, the whole attachment–detachment cycle can be separated into five stages: stage 0 occurs prior to seta–substrate contact and stages i–iv correspond to the stages labelled in figure 2*c*. In stage 0, the seta approaches the substrate until fully in contact (stage i), during which the whole ring of circular seta contacts the substrate simultaneously, whereas the spatula seta first contacts the substrate with its elongated channel portion followed by the sucker. During stage ii, the seta continues to deform until it reaches its maximum compression and completes

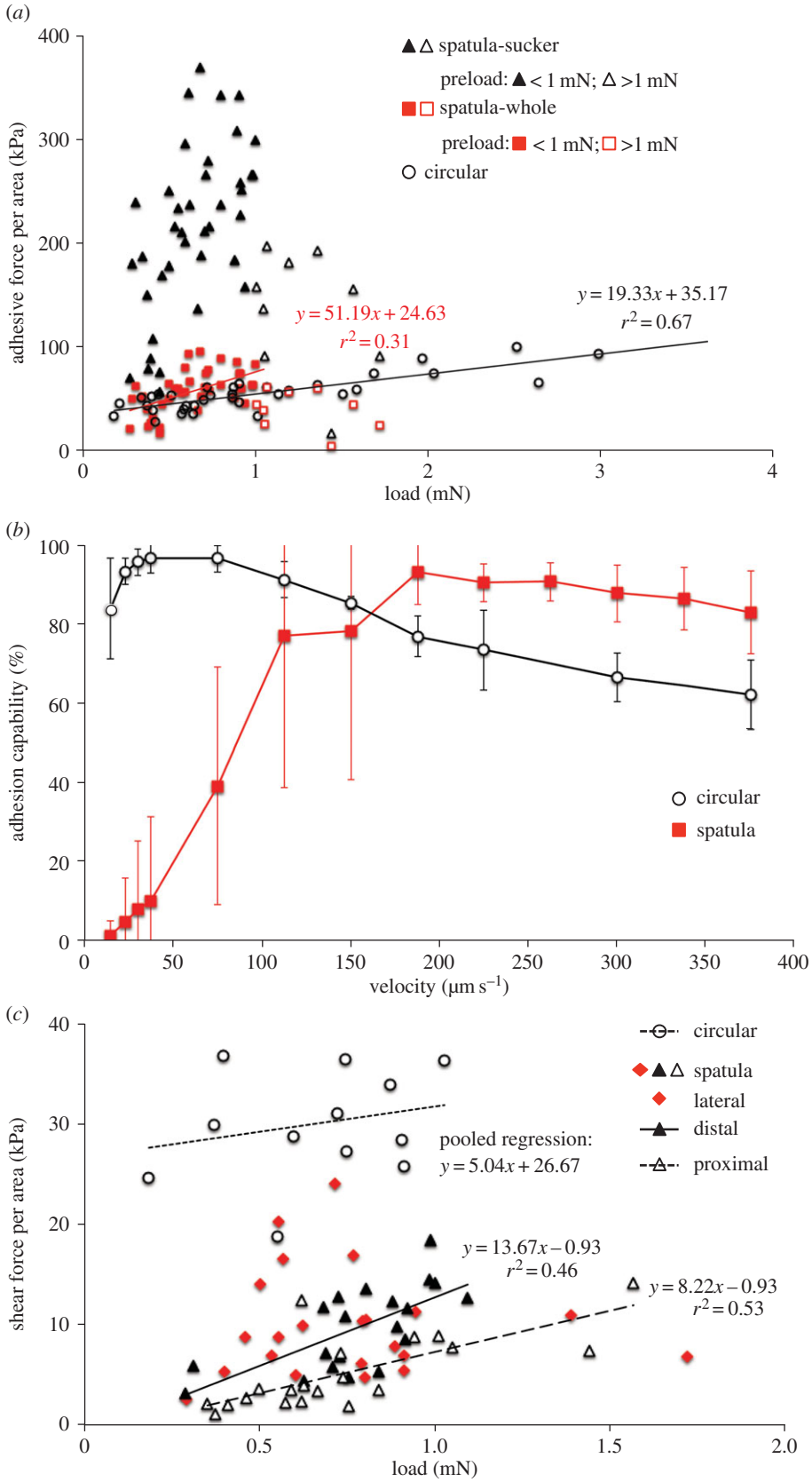

Figure 4. Attachment performance of a single seta under different conditions for circular setae from *H. pacificus* and spatula setae from *C. rugosus*. (*a*) Effects of preloading on adhesive stress of circular setae (circle; eight hairs from two subjects) and spatula setae (square: 12 hairs from six subjects). Each sample was tested under three to five preloads. Considering only the sucker area of spatula setae (triangle), the adhesive stress would become approximately four times greater. For spatula setae, filled symbols denote data under a preload of <1 mN and open symbols are for preloads >1 mN. OLS regression lines for circular setae and spatula setae at preloads of <1 mN are presented. (*b*) Effects of pull-off velocity on seta adhesion capability, quantified as the adhesive force normalized by the maximum obtained from that sample. Each symbol presents the mean with standard deviation (red square, spatula setae, $n = 6$; black circle, circular setae, $n = 5$). (*c*) Effects of preloading on the shear stress of a single seta sliding in different directions. Each sample was tested under three to four different preloads. At each preload, circular setae (circle; five hairs from two subjects) were tested in two random shearing directions and spatula setae (eight hairs from five subjects) were tested in proximal (open triangle), distal (filled triangle) and lateral (filled diamond) directions. Comparisons of OLS regression lines are presented in the electronic supplementary material table S3.

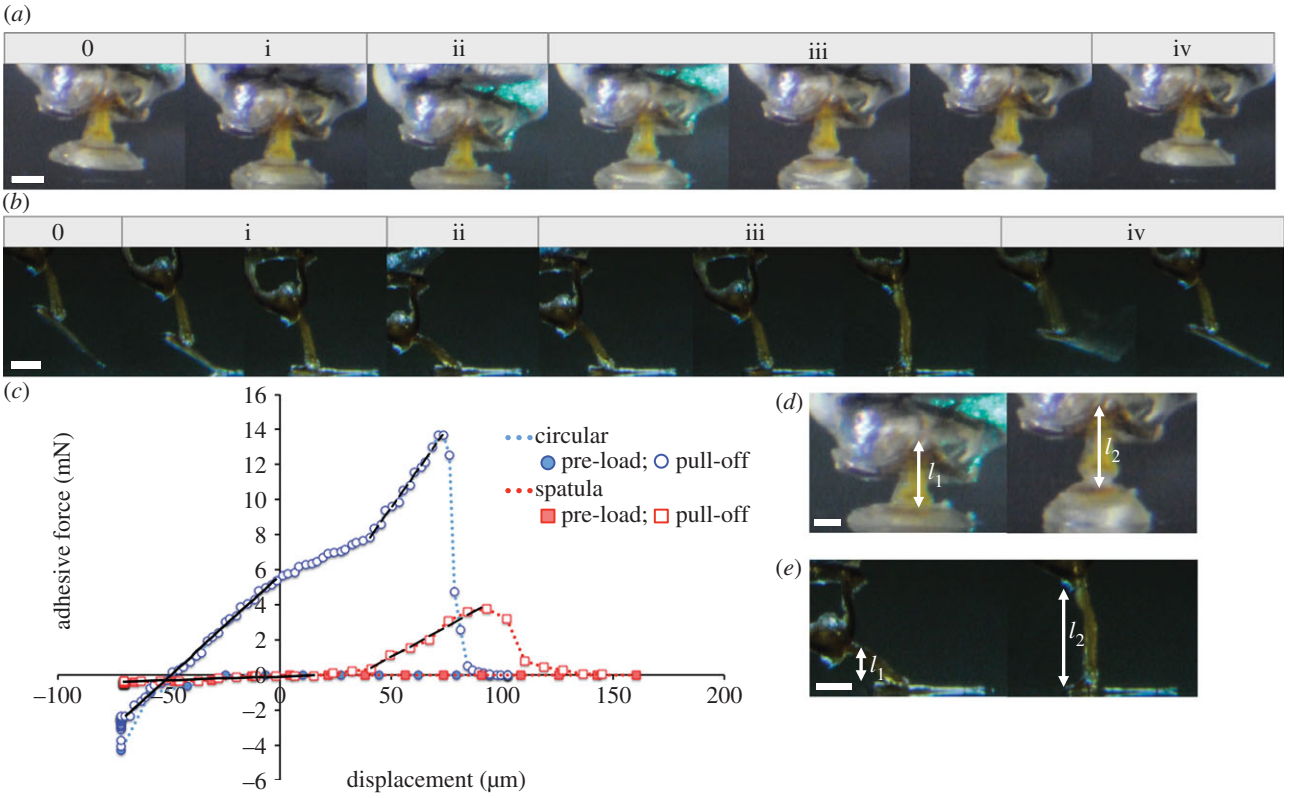

Figure 5. Attachment and detachment processes of adhesive seta from male diving beetles. (*a*) A circular seta from *H. pacificus* and (*b*) a spatula seta from *C. rugosus*. The attachment–detachment cycle can be separated into five stages. Stage 0 is the status prior to contact and stages i–iv correspond to the stages in figure 2*c*. (*c*) Force–displacement curves for circular (blue) and spatula setae (red). The seta experiences a negative force during preloading (filled symbol) and a positive force during pull-off (open symbol). Zero displacement is defined by complete seta–substrate contact during stage i. During pull-off (stage iii), spring constants for each seta are calculated as the initial (solid line) and final slopes (dashed line) of the curve. (*d–e*) Stalk heights at the beginning (l_1) and end (l_2) of the pull-off stage for a circular seta in *d* (from $l_1 \sim 270$ to $l_2 \sim 330$ μm) and a spatula seta in *e* (from $l_1 \sim 100$ to $l_2 \sim 280$ μm). The 'buffer length' is quantified as $\Delta l = l_2 - l_1$. Scale bar, 100 μm.

the attachment; that is, the sucker cup of circular setae flattens, whereas the spatula seta slides distally by bending the joints of the stalk. To firmly adhere to the substrate, the setae of either type must be pushed down to their maximum deformation. During the pull-off phase of a circular seta, the stalk and sucker both deform (stage iii) until the contact surface breaks off suddenly from the substrate (stage iv). When pulling on the spatula seta test sample, stalk rotation initially causes the stalk to slide back on the contact surface, followed by stalk extension (stage iii). The sucker–substrate contact also breaks suddenly, but the channel region peels off gradually to complete the detachment. Deformation of the spatula sucker is negligible compared with the stalk. The attachment–detachment processes for each type of seta are presented in the electronic supplementary material, movies S1–S3.

4. Discussion

4.1. Male diving beetle attachment devices: scaling and performance

In this study, we examined and compared the underwater attachment performance of two specialized adhesive setae of male diving beetles: circular suction-cup-shaped setae and spatula-shaped setae having a shallow oval sucker at their proximal bases and parallel channels running distally along the contact surface (figure 1). Although male diving beetles with both types of setae have similar body shapes and rates of increase in A_P with M_B, the palettes bearing circular setae are significantly bigger (figure 3*b* and the electronic supplementary material, table S2) and have greater total A_{ST} relative to M_B (A_{ST}/M_B approx. 11.7 $mm^2\,g^{-1}$ for circular setae, and approx. 4.8 $mm^2\,g^{-1}$ for spatula setae; tables 1 and 2). In other words, male diving beetles bearing spatula setae may have less total contact area for supporting their body weight during pre-mating courtship. Do they have a weaker attachment mechanism?

In this study, we report, for the first time, the attachment forces of a single seta from which we estimate total forces generated by a male diving beetle. Adhesion measured from two species suggests that circular and spatula setae generate similar forces per contact area (F_a/A_{ST}) of approximately 55 kPa (figure 3*c* and table 2). Provided that all setae of the two palettes are in contact with the substrate, male *C. rugosus* can generate greater total adhesion forces by having significantly more contact area than *H. pacificus* (approx. 530 versus 160 mN). However, when body weight ($BW = M_B \times g$, where g is gravitational acceleration) is taken into account, male *H. pacificus* have better adhesion performance than *C. rugosus* (total $F_a \sim 60$ versus 25 BW). Circular setae can provide significantly greater resistance to shearing stress than spatula setae, leading to a better attachment performance in *H. pacificus* males than *C. rugosus* (total $F_s \sim 35$ versus 2.5–5 BW; table 2). Compared with previous studies of whole palettes, our estimates for total adhesion are greater for both circular (60 versus 8 BW in *Dytiscus alaskanus* [36]) and spatula setae (25 versus 7 BW in *Cybister* spp. [38]). For

shear on spatula setae, however, our estimate has lower values (2.5–5 versus 19 BW in *Cybister* spp. [38]).

From an energetic perspective, we can estimate the releasing energy, which is the energy required to remove the attached sample from the substrate, by calculating the area under the force–displacement curve during the unloading (detaching) phase. The releasing energies estimated for the cases in figure 5*c* are approximately 0.14 µJ for the spatula seta and 0.9 µJ for circular seta, and when normalized by A_{ST} they are 1.9 and 3.8 µJ mm^{-2}, respectively. Consequently, it takes approximately 20 µJ to remove a 2 g male *C. rugosus* from the substrate and 10 µJ for a 0.25 g male *H. pacificus*. In summary, compared with palettes with spatula setae, those with circular setae have a relatively greater setae area and resistance to shear stress and therefore perform better when resisting pulling and sliding forces. Our results provide mechanical evidence for the advantage of using later-evolved suction-cup-shaped circular setae for underwater attachment in male diving beetles.

4.2. Force and seta deformation during attachment–detachment

Throughout the preload and pull-off processes, either type of seta performs asymmetric force–displacement responses (figure 5*c*). During the preload phase (stages i–ii in figure 5*a*,*b*), the force increases nonlinearly with deformation (dotted lines), which is mainly owing to sucker deformation in circular setae and stalk rotation in spatula setae. During the detachment (pull-off) phase (stage iii), the force remains very low in spatula setae during stalk rotation in a direction perpendicular to the substrate. Extension of the spatula stalk increases the recorded force and initiates elastic energy absorption until break-off between contact surfaces occurs. In circular setae, the recorded force increases when the stalk and sucker return to their original shape. When pulled, stalk extension and sucker deformation further increases the force and energy absorption, which leads to even greater adhesive force than spatula at break-off. In circular setae, the sudden decrease in the pull-off force is associated with the break-off between two contact surfaces after the sucker is deformed beyond its limit at the end of stage iii (figure 5*a* and the electronic supplementary material, movie S1). Although sucker deformation is rarely measured in spatula setae, similar phenomena are observed (figure 5*b* and the electronic supplementary material, movies S2 and S3). In other words, spatula setae of male diving beetles act as an effective sucker for adhesion.

Seta deformation and force–displacement (F–d) relationships suggest different mechanical behaviours between circular and spatula setae (figure 5*a*–*c*), which might have consequences in attachment performance. If we consider the whole seta as a spring, its spring constant k can be calculated as the slope of the F–d curve. The initial spring constant of spatula setae k_i is very low at approximately 5 N m^{-1}, and is mainly caused by stalk rotation until the stalk is perpendicular to the substrate. The final constant k_f, approximately 70 N m^{-1}, is much greater owing to extension of the stalk. In the circular seta, k_i is approximately 115 N m^{-1} and is caused by restoration of the sucker and stalk to their original shapes, and a greater k_f of approximately 180 N m^{-1} is associated with further deformation, mainly from the sucker. If compressive resistance has a similar magnitude to that of extension at initial pulling, the much greater k_i found in circular setae implies that a greater force is required to preload the setae before there is complete attachment. This prediction is consistent with the observation that spatula setae can adhere at significantly lower preloads (table 2 and figure 4*a*). Furthermore, the low k_i of spatula setae suggests they can adapt to differing substrates.

When a seta is subjected to a given momentum change (ΔP), the pull-off force exerted onto the contact surface is inversely proportional to the duration (Δt) of the applied force ($F = \Delta P/\Delta t$). Therefore, increased seta deformation Δl, and hence longer Δt, could lead to lower response forces. During attachment–detachment processes, both types of setae undergo similar deformations (figure 5*c*), which are, however, made by different parts of the two types of setae. During the pull-off stage, deformation in the sucker and stalk of the circular seta of *H. pacificus* is comparable (stage iii in figure 5*a*), with stalk deformation ($\Delta l = l_2 - l_1$) being approximately 60 µm (figure 5*d*). By contrast, deformation was not observed in the suckers of spatula setae of *C. rugosus*; therefore, total deformation (approx. 180 µm) is mainly contributed by the stalk through rotation and extension (figure 5*b*,*e*). Consequently, either type of adhesive seta can reduce the pull-off force experienced by the contact surface through the 'buffer length' created by seta deformation, either from the sucker and stalk of circular setae or from the stalk of spatula setae.

4.3. Direction-dependent resistance in spatula setae guides the preferred shear motion

Spatula setae exhibit direction-dependent resistance to shear, possibly owing to their asymmetrical shape and contact surface structures. Resistance is greater when sliding perpendicular to channel directions than when parallel. When a spatula seta is under a compressive preload, the contact surface shears along the substrate owing to the rotational motion at the joints of both ends of the stalk (figure 5*b* and electronic supplementary material, movie S2). When an external shear load is applied laterally, the spatula seta encounters greater resistance and the joint twists to reorient the contact surface, so that the load becomes parallel to the channel direction (electronic supplementary material, movie S4). Consequently, the sheared seta would either slide distally to complete the attachment or slide proximally prior to peel-off. Thus, the joint motion and directional difference in shear resistance could serve to guide spatula setae to move in directions that assist adhesion. Direction-dependent attachment performance has also been observed in other setae attachment mechanisms; for example, the feet of geckos [39], mayfly larvae [16], cockroaches [40], stick insects, dock beetles [41] and leaf beetles [42]. Such direction-dependence in the shear resistance of spatula setae, possibility owing to morphological symmetry, has been suggested as crucial for controlling attachment, detachment and even interaction with the substrate during their movements [12].

4.4. Velocity-dependence reveals adhesion mechanisms

Different responses to pull-off velocity in two types of setae (figure 4*b*) suggest different attachment and detachment mechanisms. The velocity-independent performance of circular setae is consistent with the use of suction (i.e. pressure differential) for adhesion. By contrast, the adhesion performance of spatula setae increases with pull-off velocity, implying a viscous force being used for adhesion as proposed for treefrog toe pads [43]. This dynamic adhesion is based on the viscous

resistance to fluid flow, which increases with fluid viscosity, contact area and flow velocity [44].

Compared with the spatula setae of terrestrial insects, those of male diving beetles have modified surface structures including a shallow concavity that might work as a sucker (discussed in §4.2.) and parallel grooves that function as water channels (figure 1). When a spatula seta is under preload, its contact surface compresses and slides distally along the substrate during which interfacial fluid volume may decrease. Under a pull-off force, the seta surface slides proximally and fluid must flow through the channels into the sucker before surface separation, and the faster the pull-off motion, the greater the generated resistance. Therefore, these grooves not only increase the effective contact area during preloading, but also create multiple flow pipes to increase viscous resistance. Consequently, when a male diving beetle mounts female elytra for pre-courtship, its spatula setae resist the female's erratic swinging motion, whereas a slow pull-off motion allows setae to detach easily.

From an evolutionary perspective, the dytiscid circular (or suction-cup) shape is a derived trait for adhesive setae, whereas the spatula shape is the primitive type [30]. Although adhesive spatula setae perform well in air by means of van der Waals and capillary forces [12], these effects deteriorate underwater [9]. Here, we present a solution provided by the spatula setae of male Cybistrini diving beetles for underwater attachment: a modified surface contact using shallow sucker and parallel channels that enables adhesion by using the combined mechanisms of suction and viscous resistance. Velocity-dependent viscous resistance from channel flow allows spatula setae to function with controllable adhesion. The 'passive suckers' of the circular setae of male diving beetles, however, create better long-term underwater adhesion without muscular control. Attachment mechanisms revealed in these two types of adhesive setae provide insights for the bioinspired design of underwater attachment devices.

5. Conclusion

Fibrillar adhesives evolved independently in several lineages of animals and have drawn much attention for their biomimetic applications. Previous studies mainly focused on their use in air involving van der Waals interactions or capillary force. Here, we report, for the first time, the functioning mechanisms of underwater attachment using the specialized adhesive hairs consisting of spatula and circular (sucker) setae found in male diving beetles. Forces and dynamics measured from setae suggest that later-evolved circular (sucker) setae working passively perform better at long-term underwater adhesion. Spatula setae with modified surface structures including a shallow sucker and channels can adhere surfaces using the combined mechanisms of suction and viscous resistance. Their velocity-dependent adhesion structures provide better control during movement and mating, and direction-dependent shear resistance helps reorient setae surfaces into preferred directions for the purpose of attachment. Seta deformation, achieved by deformation of the stalk and sucker in circular setae or by rotation and extension of the stalk in a spatula seta, reduces the force transmitted to the contact surface. The softer spring found in spatula setae explains their adhesion at lower preloading and implies easier substrate contact. Attachment mechanisms revealed in adhesive dytiscid modified spatula and passive sucker setae provide insights for bioinspired designs of underwater attachment devices.

Acknowledgements. We are grateful to the following people and institutions. For the initial idea and help in locating collecting sites: C.-Y. Tsai (Wu-Ling Senior High School); for assistance and discussion on experiments and results: J.-R. Roan, M.-H. Lee and K.-B. Chen; for assistance and advice on diving beetles, M.-L. Jeng (National Museum of Natural Science, NMNS), L.-J. Wang (Taiwan Agricultural Research Institute, TARI), S.-W. Hou, K. J. Liu, H.-W. Hsieh (National Taiwan University, NTU), C.-R. Chen and J.-R. Jheng; for assistance with museum specimens, M.-L. Chan and H.-H. Liang (NMNS); for assistance with the SEM, W.-J. Jian and T.-S. Wang (NTU). We also thank the anonymous referees for helpful comments and suggestions. This study benefited from discussions with members of the NCHU Shih-Roan-Chi biophysics group and the Complexity and Life Focus Group supported by the National Centre of Theoretical Sciences (NCTS) of Taiwan.

Funding statement. This study was funded by the National Science Council (NSC) of Taiwan to K.-J.C. (grant no. 99-2112-M-005-004).

References

1. Nachtigall W. 1974 *Biological mechanisms of attachment: the comparative morphology and bioengineering of organs for linkage, suction, and adhesion*. New York, NY: Springer.
2. von Byern J, Wani R, Schwaha T, Grunwald I, Cyran N. 2012 Old and sticky: adhesive mechanisms in the living fossil *Nautilus pompilius* (Mollusca, Cephalopoda). *Zoology* **115**, 1–11. (doi:10.1016/j.zool.2011.08.002)
3. Smith AM. 2002 The structure and function of adhesive gels from invertebrates. *Integr. Comp. Biol.* **42**, 1164–1171. (doi:10.1093/icb/42.6.1164)
4. Betz O, Kölsch G. 2004 The role of adhesion in prey capture and predator defence in arthropods. *Arthropod Struct. Dev.* **33**, 3–30. (doi:10.1016/j.asd.2003.10.002)
5. Gorb SN. 2010 Biological and biologically inspired attachment systems. In *Springer handbook of nanotechnology* (ed. B Bhushan), pp. 1525–1551. New York, NY: Springer.
6. Gorb S. 2001 *Attachment devices of insect cuticle*. Boston, MA: Kluwer Academic Publishers.
7. Gorb SN. 2008 Biological attachment devices: exploring nature's diversity for biomimetics. *Phil. Trans. R. Soc. A* **366**, 1557–1574. (doi:10.1098/rsta.2007.2172)
8. Autumn K, Liang YA, Hsieh ST, Zesch W, Chan WP, Kenny TW, Fearing R, Full RJ. 2000 Adhesive force of a single gecko foot-hair. *Nature* **405**, 681–685. (doi:10.1038/35015073)
9. Lee H, Lee BP, Messersmith PB. 2007 A reversible wet/dry adhesive inspired by mussels and geckos. *Nature* **448**, 338–342. (doi:10.1038/nature05968)
10. Geim AK, Dubonos SV, Grigorieva IV, Novoselov KS, Zhukov AA, Shapoval SY. 2003 Microfabricated adhesive mimicking gecko foot-hair. *Nat. Mater.* **2**, 461–463. (doi:10.1038/nmat917)
11. Spolenak R, Gorb S, Gao H, Arzt E. 2005 Effects of contact shape on the scaling of biological attachments. *Proc. R. Soc. A* **461**, 305–319. (doi:10.1098/rspa.2004.1326)
12. Gorb SN. 2011 Biological fibrillar adhesives: functional principles and biomimetic applications. In *Handbook of adhesion technology* (eds LFM da Silva, A Öchsner, RD Adams), ch. 54, pp. 1409–1436. New York, NY: Springer.
13. Gorb SN, Varenberg M. 2007 Mushroom-shaped geometry of contact elements in biological adhesive systems. *J. Adhes. Sci. Technol.* **21**, 1175–1183. (doi:10.1163/156856107782328317)
14. Scherge M, Gorb SN. 2001 *Biological micro- and nanotribology: nature's solutions*. New York, NY: Springer.

15. Varenberg M, Pugno NM, Gorb SN. 2010 Spatulate structures in biological fibrillar adhesion. *Soft Matter* **6**, 3269–3272. (doi:10.1039/c003207g)
16. Ditsche-Kuru P, Koop JHE, Gorb SN. 2010 Underwater attachment in current: the role of setose attachment structures on the gills of the mayfly larvae *Epeorus assimilis* (Ephemeroptera, Heptageniidae). *J. Exp. Biol.* **213**, 1950–1959. (doi:10.1242/jeb.037218)
17. Waite JH. 1987 Nature's underwater adhesive specialist. *Int. J. Adhes. Adhesives* **7**, 9–14. (doi:10.1016/0143-7496(87)90048-0)
18. Smith AM. 1991 Negative pressure generated by octopus suckers: a study of the tensile strength of water in nature. *J. Exp. Biol.* **157**, 257–271.
19. Smith AM. 1996 Cephalopod sucker design and the physical limits to negative pressure. *J. Exp. Biol.* **199**, 949–958.
20. Tramacere F, Beccai L, Kuba M, Gozzi A, Bifone A, Mazzolai B. 2013 The morphology and adhesion mechanism of *Octopus vulgaris* suckers. *PLoS ONE* **8**, e65074. (doi:10.1371/journal.pone.0065074)
21. Tramacere F, Kovalev A, Kleinteich T, Gorb SN, Mazzolai B. 2014 Structure and mechanical properties of *Octopus vulgaris* suckers. *J. R. Soc. Interface* **11**, 20130816. (doi:10.1098/rsif.2013.0816)
22. Geerinckx T, Herrel A, Adriaens D. 2011 Suckermouth armored catfish resolve the paradox of simultaneous respiration and suction attachment: a kinematic study of *Pterygoplichthys disjunctivus*. *J. Exp. Zool. A, Ecol. Genet. Physiol.* **315**, 121–131. (doi:10.1002/jez.656)
23. Kemp PS, Tsuzaki T, Moser ML. 2009 Linking behaviour and performance: intermittent locomotion in a climbing fish. *J. Zool.* **277**, 171–178. (doi:10.1111/j.1469-7998.2008.00525.x)
24. Motta PJ, Fulcher BA. 2006 Suction disk performance of echeneid fishes. *Can. J. Zool.* **84**, 42–50. (doi:10.1139/z05-167)
25. Varenberg M, Gorb S. 2008 A beetle-inspired solution for underwater adhesion. *J. R. Soc. Interface* **5**, 383–385. (doi:10.1098/rsif.2007.1171)
26. Heepe L, Varenberg M, Itovich Y, Gorb SN. 2011 Suction component in adhesion of mushroom-shaped microstructure. *J. R. Soc. Interface* **8**, 585–589. (doi:10.1098/rsif.2010.0420)
27. Arnett RH, Thomas MC. 2001 *American beetles*. Boca Raton, FL: CRC Press.
28. Grimaldi DA, Engel MS. 2005 *Evolution of the insects*. Cambridge, UK: Cambridge University Press.
29. Aiken RB. 1992 The mating behavior of a boreal water beetle, *Dytiscus alaskanus* (Coleoptera, Dytiscidae). *Ethol. Ecol. Evol.* **4**, 245–254. (doi:10.1080/08927014.1992.9523136)
30. Miller KB. 2003 The phylogeny of diving beetles (Coleoptera: Dytiscidae) and the evolution of sexual conflict. *Biol. J. Linn. Soc.* **79**, 359–388. (doi:10.1046/j.1095-8312.2003.00195.x)
31. Schulte-Hostedde A, Alarie Y. 2006 Morphological patterns of sexual selection in the diving beetle *Graphoderus liberus*. *Evol. Ecol. Res.* **8**, 891–901.
32. Darwin C. 1871 *The descent of man and selection in relation to sex*. London, UK: John Murray.
33. Karlsson Green K, Kovalev A, Svensson EI, Gorb SN. 2013 Male clasping ability, female polymorphism and sexual conflict: fine-scale elytral morphology as a sexually antagonistic adaptation in female diving beetles. *J. R. Soc. Interface* **10**, 20130409. (doi:10.1098/rsif.2013.0409)
34. Bergsten J, Töyrä A, Nilsson AN. 2001 Intraspecific variation and intersexual correlation in secondary sexual characters of three diving beetles (Coleoptera: Dytiscidae). *Biol. J. Linn. Soc.* **73**, 221–232. (doi:10.1111/j.1095-8312.2001.tb01359.x)
35. Bergsten J, Miller KB. 2007 Phylogeny of diving beetles reveals a coevolutionary arms race between the sexes. *PLoS ONE* **2**, e522. (doi:10.1371/journal.pone.0000522)
36. Aiken RB, Khan A. 1992 The adhesive strength of the palettes of males of a boreal water beetle, *Dytiscus alaskanus* J. Balfour Browne (Coleoptera: Dytiscidae). *Can. J. Zool.* **70**, 1321–1324. (doi:10.1139/z92-185)
37. Yang Z, Dai Z, Wang W. 2009 Morphology and adhesive characteristics of Cybister (male) fore-foot adhesive pads. (In Chinese). *Acta Mater. Comp. Sin.* **26**, 213–218.
38. Wang W, Dai Z, Yu Q, Yang Z. 2007 Ultrastructure and adhesive strength of adhesive discs of diving beetles. (In Chinese). *J. Nanjing Univ. Aeronaut. Astronaut.* **39**, 75–79. (doi:10.3969/j.issn.1005-2615.2007.01.016)
39. Gravish N, Wilkinson M, Autumn K. 2008 Frictional and elastic energy in gecko adhesive detachment. *J. R. Soc. Interface* **5**, 339–348. (doi:10.1098/rsif.2007.1077)
40. Clemente CJ, Federle W. 2008 Pushing versus pulling: division of labour between tarsal attachment pads in cockroaches. *Proc. R. Soc. B* **275**, 1329–1336. (doi:10.1098/rspb.2007.1660)
41. Clemente CJ, Bullock JM, Beale A, Federle W. 2010 Evidence for self-cleaning in fluid-based smooth and hairy adhesive systems of insects. *J. Exp. Biol.* **213**, 635–642. (doi:10.1242/jeb.038232)
42. Voigt D, Schweikart A, Fery A, Gorb S. 2012 Leaf beetle attachment on wrinkles: isotropic friction on anisotropic surfaces. *J. Exp. Biol.* **215**, 1975–1982. (doi:10.1242/jeb.068320)
43. Smith J, Barnes W, Downie J, Ruxton G. 2006 Structural correlates of increased adhesive efficiency with adult size in the toe pads of hylid tree frogs. *J. Comp. Physiol. A* **192**, 1193–1204. (doi:10.1007/s00359-006-0151-4)
44. Denny MW. 1993 *Air and water: the biology and physics of life's media*. Princeton, NJ: Princeton University Press.